12-13-2017

A Physical Framework for Evaluating Flood Inundation Risk Under Different Water Management Scenarios

sage hardesty
sage.hardesty@uconn.edu

A Physical Framework for Evaluating Flood Inundation Risk Under Different Water Management Scenarios

Sage Hardesty

B.S., University of Delaware, 2014

A Thesis

Submitted in Partial Fulfillment of the

Requirements for the Degree of

Master of Science

At the

University of Connecticut

2017

APPROVAL PAGE

Masters of Science Thesis

A Physical Framework for Evaluating Flood Inundation Risk Under Different Water Management Scenarios

Presented by

Sage Hardesty, B.S.

Major Advisor_____
Emmanouil Anagnostou

Associate Advisor_____
Guiling Wang

Associate Advisor_____
Xinyi Shen

University of Connecticut

2017

ACKNOWLEDGEMENTS

I would like to thank my M.S. academic advisor E. N. Anagnostou for his advice, patience, and assistance throughout my time at UCONN. I would like thank X. Shen for continued support with everything technical within my research. I would also like to thank my committee member G. Wang.

I would like to thank Jason Parent and Dave Wanik for supplying the Connecticut LIDAR terrain elevation data. I would like to thank Rachel Lonchar and Gabriella Pagliuca for help during the initial development of the HEC-RAS model. I would also like to thank Amy Charlton and engineers at the Thomaston Dam for providing the necessary construction information to create the dam model.

Finally, I would like to thank my family for keeping me grounded, present, and focused on my goals.

Table of Contents

Abstract

In the United States, many river floodplains contain critical infrastructure that is vulnerable to extreme hydrologic events. These structures are designed based on flood frequency analysis aimed at quantifying the magnitude of the extreme events. However, many floodplains are ungauged or poorly gauged, making flood frequency analysis significantly uncertain. This research topic focuses on estimating flood frequency peaks for an ungauged critical infrastructure within Connecticut's Naugatuck River Basin utilizing a physically based approach consisting of a distributed rainfall-runoff model forced by long-term reanalysis meteorological data and a hydraulic model driven by high-resolution LiDAR derived terrain elevation data. The hydrologic model reanalysis is used to derive 50-, 100-, 200-, and 500-year return period flood peaks, which are then used to drive one-dimensional HEC-RAS unsteady hydraulic model to estimate the inundation risk of a sub-station and evaluate hydraulic structure operation strategies to reduce inundation risk of the downstream infrastructure. This study illustrates the potential of the physically based approach to creating flood maps in an ungauged basin and demonstrates the effects of different water management scenarios on the flood risk of the downstream infrastructure.

1. Introduction

Floods are among the most damaging natural disasters, with increasing impact and frequency. In the United States alone in recent decades floods have accounted for thousands of deaths and tens of billions of dollars in annual losses (Hirabayashi et al., 2013). Additionally, many utilities rely on critical infrastructure located in floodplains that are vulnerable to these extreme hydrologic events, allowing disturbances to extend beyond the floodplain. In flood resilience**,** we seek to quantify and mitigate the flood risk, as well as expediate recovery from the consequences after a flooding event occurs (Schinke et al, 2016). Resilience can be improved in many ways, including: land use management, flood infrastructure management and operation, storm water withholding, more effective flood emergency preparedness, and flood response policy. However, before policy actions can be put in place, the risk must first be systematically quantified.

In relation to flood design, engineers use frequency analysis to transform historical flow observations into future flood occurrences, by relating the magnitude of a flood event to the frequency of its occurrence through probability distribution. Flood frequency distributions come in many forms, however Log-Pearson Type III is recommended by the U.S. Water Resource Council (U.S. Water Resources Council, 1981). The relation between flow rate and frequency of occurrence at any streamflow gauging station is typically expressed by means of exceedance probability or recurrence interval. Exceedance probability is the likelihood that a stream would experience a given flow rate in any year. Recurrence interval is the average amount of time (in years) expected to pass before a stream experiences a given flow rate one time. While this

relationship is built from long historic records, they are not finite predictive measures. They only express the statistical probability of occurrences (Ahearn et al., 2009). Nevertheless, information regarding magnitude and frequency of occurrence of flooding events gathered through flood frequency analysis (FFA) is instrumental to mitigating losses associated with future floods, particularly when designing hydraulic structures such as reservoirs and dams. However, rarely do areas of interest coincide with a stream gage. It is often difficult to implement FFA in ungauged or poorly gauged basins because they lack the necessary long-term streamflow records; less than 10% of the 250,000 rivers in the United States are gauged daily by the USGS (Geological Survey, 2009).

Hydrologists have developed a number of methods to conduct FFA in ungauged basins lacking sufficient data. These methods can broadly be classified into two groups: statistical approaches and rainfall-runoff modeling. For statistical approaches, statistical analysis or hydrological regionalization are used to transfer hydrological information from one or more homogenous gauged catchments to a neighboring or geographically/ hydrologically similar ungauged basin (Bao et al., 2012; Razavi and Coulibaly, 2012; Loukas and Vasiliades, 2014; Xiong et al., 2015). However, the quality of the estimation in the ungauged basin is subject to the continuous length of flow observations of the neighbor gauged basins, and potential nonstationarity of the historical flood trend. In an alternate approach, observed precipitation combined with various other meteoritical forcing parameters are used to drive physically-based hydrologic and flood routing models to simulate surface flows in ungauged basins. Surface flows are made up of both overland and channel flow routing, which can either be handled separately by two models (Julien et al., 1995; Qu and Duffy, 2007), or combined through a coupled model (Cea et al., 2010; Kim et al., 2012). This study used The Coupled Routing and Excess Storage-

Soil-Vegetation-Atmosphere-Snow (CREST-SVAS) model to simulate flows in ungauged basins of Northeastern United States (Shen and Anagnostou, 2017). Hydrodynamic routing models simulate surface flows based on solutions to simplified shallow water equations like: the kinematic wave (Vivoni et al., 2007) or diffusion wave equations (Qu and Duffy, 2007). Solutions to these equations rely on parameters directly derived from physical watershed characteristics rather than empirically estimated coefficients. Specifically, physically-based distributed hydrologic models are able to capture the spatial variability of hydrologic parameters, thereby better characterize the heterogeneity of certain complex hydrologic processes within ungauged catchments (Wang et al., 2011; Shen and Anagnostou, 2017; Li et al., 2015). In inland watersheds flooding is caused by rainfall, snowmelt, or a combination of both. Distributed hydrologic models have the capacity of accounting for the intra-basin variability of runoff-producing mechanisms by digesting gridded meteorological forcing, remote sensing, terrain and soil data. Furthermore, with the availability of re-analysis forcing datasets like the North American Land Data Assimilation System (NLDAS), hydrologic models can now make use of quality controlled, temporally and spatially consistent datasets at a fine spatiotemporal resolution, often in areas that were previously uncovered by ground-based measurement networks.

To further quantify flood risk and identify flood prone areas, a hydraulic model (one-dimensional or two-dimensional) is used to simulate the spatial distribution of hydraulic variables like water depth and flood inundation extent. For efficiency considerations, the Army Corps of Engineers' developed Hydrologic Engineering Center's River Analysis System (HEC-RAS) hydraulic model was used to perform one-dimensional unsteady flow calculations, and to simulate water surface profiles. Two main forcing factors are required in HEC-RAS: the flood

event's streamflow time-series and bathymetry of the river channel and surrounding floodplain. HEC-RAS is fully compatible with ArcGIS and accepts vector and raster data formats, therefore, the model gains access to one or two-dimensional representations of measured/computed hydraulic parameters at a fine spatial scale. High-resolution topographic data is necessary to capture the finer-scale heterogenous features of a river and its floodplain and their effects on flood propagation. LIDAR provides topography at a finest resolution (1m) over regional scale. Simulation accuracy is sensitive to DEM resolution. This improvement in resolution directly translates to the model's ability to accurately map flood inundation extent. (Cook et al. 2009) demonstrated that for a given flow and geometric description, HEC-RAS model predicted inundated area decreased by 25% when forced with 6 m LIDAR DEM instead of the 30 m National Hydrographic Dataset (NHD).

The objective of this study is to further improve flood vulnerability assessment in ungauged regions with a physically based methodology (Figure 1) and demonstrate it over a case study in the Naugatuck River of Connecticut. Specifically, peak flows of the Naugatuck River were simulated using the CREST-SVAS model forced with long-term (35 years) atmospheric re-analysis data. Flood frequencies with 0.02, 0.01, 0.005, and 0.002 exceedance probabilities (50, 100, 200, and 500 return year periods, respectively) were estimated by fitting the Pearson Type III distribution. These peak flows were then used to construct synthetic hydrographs using a methodology proposed by Archer (2000). Based on LIDAR derived high resolution DEM, these synthetic hydrographs forced HEC-RAS to generate flood inundation maps in a region controlled by a dam. This study's CREST-SVAS runoff simulations exhibited good agreement with stream flow measurements from an upstream USGS station, and HEC-RAS one-dimensional modeling

approach exhibited good agreement with measured stage-discharge ratings based on one of the most severe historic events in our database.

The following section includes a description of the study area and of the included critical infrastructure and flood control structure. Section 3 describes the LIDAR high-resolution terrain elevation data and the long-term meteorological forcing data used in this study. Section 4 explains the proposed methodology of simulating synthetic stream flows in ungauged basins, conducting frequency analysis, creating a synthetic hydrograph and mapping flood inundation through use of the herein described models. In section 5 we present our models' validation. Flood inundation results for the case study are presented in section 6, followed by closing remarks in section 7.

2. Study Area

Located in Western Connecticut, the Naugatuck River is the largest tributary of the Housatonic River. Entirely confined within the state's borders, the Naugatuck River spans over 39 miles south from Torrington to Derby, 12 miles north of the Long Island Sound. The stream features quick flows for the majority of its length, due to its fairly steep gradient of 13 feet per mile. This steep gradient causes the runoff from precipitation in the basin to be rapid, and leaves the river prone to flooding. In this study basin, the greatest floods generally occur in the spring, where heavy rainfall can trigger snowmelt which then contributes significantly to the flood magnitude and volume. Previous models have failed to capture flood peaks in this region due to the complexities of this hydrologic interaction (Dis et al., 2015; Parr et al., 2015). At its outlet, the river has an average annual streamflow on the order of 560 cubic feet per second (cfs), while

minimum baseflows are approximately 80 cfs. The river's watershed is an approximate 311 square miles covering portions of 27 different towns. The watershed contains a variety of land uses, including but not limited to: rural, dense urban, suburban, agricultural, and undeveloped forested areas (http://naugawatshed.org/).

For this study two separate river reaches were selected to investigate, primarily because of the presence of critical infrastructure in these areas. One infrastructure, just a mile north to Thomaston, and at approximately the midway point of the Naugatuck River is the Thomaston Dam. A flood control dam built and operated by the U.S. Army Corps of Engineers in 1960, the Thomaston Dam is a 142-feet high, 2000 feet long, horseshoe shaped earth fill dam with two 10 feet adjustable gates. While the Dam is normally empty, it has the potential to utilize 960 acres to store up to 13.7 billion gallons of water (http://www.nae.usace.army.mil). The other critical infrastructure, an electrical substation is located in Waterbury, perhaps the most urbanized and industrialized portion of the river and only 9 miles downstream of the Dam. This electrical substation features both an enclosed building complex as well as outside transformers, both in close proximity to the Naugatuck River (Figure 2c).

Within the context of this study, the Naugatuck River Basin was split into two sub-basins, with the dividing point located at the Thomaston Dam (Figure 2b). The upstream portion will henceforth be referred to as river reach "A", and the downstream portion being river reach "B." This separation was done to help isolate streamflow contributions at the outlet of the dam from contributions of overland runoff, and thus attempting to re-create the influence of dam regulations on downstream floodplains. For validation purposes simulated flows were compared to the only USGS steam gage in the area located upstream (USGS 01206900) in the Naugatuck River at Thomaston, CT (Figure 2a) as well as a stream gage at the inlet of the Thomaston dam.

3. Description of Data

LIDAR Terrain Elevation Data

Accurate hydraulic simulations rely on high resolution digital terrain models (DTMs) to profile channel topography and floodplain elevation data over large regions. The accuracy of these DTMs or Digital Elevation Models (DEMs) directly influence the accuracy of inundation mapping (Coveney, 2011). Recent advancements in airborne Light Detection and Ranging (LIDAR) have led it to become the more efficient, cost-effective, and accurate terrain elevation technique in comparison to other land survey techniques. Through the combined use of a Global Positioning System (GPS), Inertial Measuring Unit (IMU), light-emitting scanning scanner, and post processing procedures, a high accurate mass point cloud dataset is produced that can be analyzed through Geographic Information Systems (GIS) like ArcGIS to generate a high-resolution three-dimensional digital terrain model.

For this study, LIDAR data was provided by Connecticut Environmental Conditions Online (CTECO). The LIDAR data is available statewide, representing approximately 5,240 square miles in the form of USGS Quality Level 2, and point density of 2 points per square meter, hydro-flattened bare earth 1m resolution. The LIDAR flights took place between March 11, and April 16, 2016. These flights occurred during a low flow season when the depth of the river's water can be considered negligible compared to water depths during flood events. The horizontal datum is North American Datum of 1983 (NAD83 2011) and the vertical datum is North American Vertical Datum of 1988 (NAVD88). The LIDAR surface was evaluated using a collection of 181 GPS surveyed checkpoints, and produced an average vertical error of 0.0012192 meters with a standard deviation of 0.0695 meters (http://cteco.uconn.edu).

However, LIDAR is still subject to its own errors. Streambed profiles measured through LIDAR techniques tend to be incorrect. This is due to the backscatter effect, the inability of LIDAR pulse to penetrate water surfaces. These uncertainties have the potential to propagate, leading to an underestimation of water held in the stream channel, or an overestimation of water in the surrounding floodplain. In an investigation done by Hilldale et al. (2007) on the accuracy of LIDAR bathymetry for the Yakima River in Washington State, mean vertical errors between remotely sensed and survey data were in the range of 0.10 and 0.27 meters, with standard deviations from 0.12 to 0.31 m. Nevertheless, LIDAR DEMs have enormous potential for application in various areas including land-use planning, management and hydrologic modelling. Specifically, in regards to hydraulic modeling, making using of a fine-resolution LIDAR based DEM profiles of stream cross-sections at critical locations with the closest spacing moves the model set-up towards being more spatially distributed in nature, likely resulting in performance improvements.

NLDAS Reanalysis Forcing Data

The North American Land Data Assimilation System(NLDAS-2) is a collaborative project involving several groups: NOAA/NCEP's Environmental Modeling Center (EMC), NASA's Goddard Space Flight Center (GSFC), Princeton University, the University of Washington, the NOAA/NWS Office of Hydrological Development (OHD), and the NOAA/NCEP Climate Prediction Center (CPC).

The NLDAS reanalysis dataset is in $1/8^{th}$-degree grid resolution, hourly temporal resolution, and is available from January 1^{st}, 1979 to present day. The non-precipitation land-surface forcing fields are derived directly from the analysis fields of NARR. The precipitation

field in NLDAS results from a temporal disaggregation of a gauge-only CPC analysis of daily precipitation over the continental United States (Higgins et al. 2000). This analysis is performed directly on the NLDAS 1/8th-degree grid, and includes an orographic adjustment stemming from the long-established PRISM climatology (Daly et al. 1994). The hourly disaggregation weights for this precipitation field are derived from either 8-km CMORPH hourly precipitation analyses (Higgins et al., 2000), NARR-simulated precipitation, or WSR-88D Doppler radar-based precipitation estimates (Baldwin and Mitchell, 1997).

4. Description of Methods

CREST-SVAS Hydrologic Model

This study utilized the newest Coupled Routing and Excess STorage model, version 3.0 with soil-vegetation-atmosphere-snow extension (CREST-SVAS) (Shen and Anagnostou, 2017). CREST-SVAS is a computationally efficient, fully distributed hydrological model designed to simulate flow discharges for large watersheds at a fine spatiotemporal resolution (30 m to 1 km spatial grid resolution and hourly time steps). CREST-SVAS integrates a runoff generation module to simulate vertical fluxes with a routing module to simulate channel discharge at each time step. The runoff generation model couples energy and water balances in four different medium: atmosphere, canopy, snow pack and layered soil, by solving water and energy balances coupled equations simultaneously. It takes dynamic (precipitation, radiation, humidity, wind speed, leaf area index) and static (land cover, soil properties, impervious ratios) input variables. Due to its strong physical basis and computational efficiency, CREST-SVAS is capable of producing long term, high-resolution hydrological simulations at various basin scales and types.

By physically coupling the snow accumulation/ablation with other water cycle processes in the SVA structure, CREST-SVAS gains improved simulation accuracy in situations previously considered difficult basins with mixed phase precipitation (Shen and Anagnostou 2017).

Flood Frequency Analysis Method –LPIII

Peak-flow frequency analysis is the process of evaluating peak magnitudes and frequencies of past floods in order to estimate the exceedance probabilities of similar floods in the future. This probability information is vital to the accurate delineation of flood zones and safe design of hydraulic structures (Ahearn, 2003). Bulletin #17B of the U.S. Water Resource Council recommends Log-Pearson Type III as the statistical distribution technique to determine peak-flow frequency estimates. Log-Pearson Type III utilizes three statistical parameters: the mean, standard deviation, and skew coefficient to describe the theoretical distribution of the peak-flow data (U.S. Water Resources Council, 1981). Previous work has been performed by Chow (1951) to demonstrate that stream flow rates in m^3/s (Q) for various probability distributions can be calculated for specific flood return periods through Eq. (1).

$$LogQ = \overline{Q_l} + K_T S_l \tag{1}$$

$\overline{Q_l}$ is the mean of the logarithms of the annual peak flow, S_l represents the standard deviation of logarithms of the annual peak flows, and K_T is the frequency factor of annual exceedance probability for return period (T) presented in Table 7.7 of Haan (1977). These K_T values are for Log-Pearson Type III with accompanying skew coefficients (C_S) which can be calculated through Eq. (2):

$$C_S = \frac{n\sum_{i=1}^{n}(Q_{l_1} - \overline{Q_l})^3}{(n-1)(n-2){S_l}^3} \tag{2}$$

In this case n is the number of values in the peak-flow dataset and i is the individual time step.

Careful consideration must be used when deleting outliers from already small samples sizes, as 10 years of flow observations is the minimum recommended threshold for determining peak-flow frequency estimates (Chow, et al., 1988). The following equation (3) serves to identify high (Q_{High}) and low (Q_{Low}) outliers.

$$logQ_{High(Low)} = \overline{Q_l} \pm K_n S_l \quad (3)$$

K_n is a outlier test frequency value and is tabulated according to sample size (U.S. Water Resources Council, 1981). One sided tests are used to determine whether outliers exist at the 10-percent confidence level for normally distributed data. Following the Water Resources Council's (WRC) method, if any of the peaks in a sample are greater or smaller than Q_{High} or Q_{Low}, respectively, they are considered outliers and deleted prior to performing the frequency analysis.

The skew coefficient used to modify the Log-Pearson Type III distribution is extremely sensitive for small samples thus further emphasis is placed on the importance of sample size. In order to improve estimation accuracy, the WRC recommends using a weighted skew coefficient (C_w). Eq. (4) combines the computed station skew coefficient (C_s) and the generalized map skew coefficient (C_m) to calculated (C_w) (Tasker, 1978). The generalized map skew coefficient can be determined from the Plate I map in Bulletin #17B of the U.S. Water Resources Council (1981).

$$C_{W=\frac{V(C_m)C_S+V(C_S)C_m}{V(C_m)+V(C_S)}} \quad (4)$$

$V(C_m)$ and $V(C_s)$ represent variances for generalized and station skew coefficients respectively. The WRC recommends a $V(C_m)$ value of 0.302 for the continental United States

when generalized skews are selected from the Plate I map in Bulletin #17B. Furthermore, the variance of the station skew V(C_s) for Log-Pearson Type III random variables and be appropriately approximated by equation (5) in agreement with results of Monte Carlo experiments performed by Wallis et al. (1974) (Chow, et al., 1988).

$$V(C_s) = 10^{A - B\log_{10}(\frac{n}{10})} \tag{5}$$

For the equation above:

$$A = \{-0.33 + 0.08|C_s| \quad \text{if} \ \ |C_s| \leq 0.90\} \tag{6}$$
$$A = \{-0.52 + 0.30|C_s| \quad \text{if} \ \ |C_s| > 0.90\}$$

And

$$B = \{0.94 - 0.26|C_s| \ \ \text{if} \ \ |C_s| \leq 1.50\}$$
$$B = \{0.55 \quad \text{if} \ \ |C_s| > 1.50\} \tag{7}$$

It is important to include confidence intervals complying with the confidence level (β) or significance level (α=(1-β)/2) when presenting statistical estimates. The 50 and 90 percent confidence limits for the 20, 50, 100, 200, and 500-year return period discharge for the Naugatuck River Basin were calculated via Eq. (8):

$$U(L)_{T,\alpha} = \overline{Q_l} \pm K_{T\alpha}^{U(L)} S_l \tag{8}$$

$K_{T\alpha}^{U(L)}$ represents for the upper (lower) confidence limit factor needed to calculate the upper (lower) limit logarithmic flow discharge $U_{T,\alpha}\left(L_{T,\alpha}\right)$. The aforementioned factors were approximated using Eqs. (9) and (10) (U.S. Water Resources Council, 1981):

$$K_{T,\alpha}^{U(L)} = \frac{K_T \pm \sqrt{{K_t}^2 - ab}}{a} \quad (9)$$

where

$$a = 1 - \frac{{Z_\alpha}^2}{2(n-1)} \text{ and } b = {K_T}^2 - \frac{{z_\alpha}^2}{n} \quad (10)$$

Z_α is the standard normal variable with exceedance probability α..

Adjustment Technique for Flood Frequency Estimation

As introduced earlier, gridded forcing data of 1/8th-degree (~14km) spatial resolution is used in this study to force CREST. In practice, most meteorologic forcing data sacrifice their spatial resolution to obtain relatively high temporal resolution (hourly to daily). Local extreme precipitation is almost always smoothed. Consequently, it is commonly to expect that the simulated flow peak cannot fully capture the reality. In other words, underestimating flood peaks constantly exists, which undermines the estimation of flood frequency. To address such underestimation, we proposed an adjusting technique to post process CREST flow output only to improve the quality of flood frequency estimation. Since the frequency estimation depends solely on annual peak of the flow time series, only the top ranked flow rate will affect this estimation, we only adjust top percentiles values using **Error! Reference source not found.**.

$$Q^{obs}(p) = a\left[Q^{sim}(p)\right]^b, p \geq p_0 \quad (11)$$

where $Q^{obs}(p)$ and $Q^{sim}(p)$ stand for observed and simulated flow at p percentile and p_0 is the lowest percentile of all annual peaks. Equation **Error! Reference source not found.** is

established on stable relationship of top ranked flow value between observation and simulation. In practice, such relationship is stable over almost all hydrologic gauges.

Constructing Synthetic Hydrograph

Flood frequency analysis only gives flood peak magnitude information. Realistic unsteady scenarios require a complete hydrograph rather than assuming a constant flow using the peak value for the flood event period. There are multiple proposed methodologies that combine statistical properties of rainfall events with a deterministic model of catchment behavior, thereby standardizing dynamic catchment behaviors. These methods, like the Soil Conservation Service (SCS) (USDA, 1986) method in the United States or the Flood Studies Rainfall Runoff (FSR) (NECR, 1975) method in the UK, create design hydrographs based on the following parameters: a design rainfall amount, duration and profile, a percentage runoff based on static and dynamic characteristics of a basin a unit hydrograph parameterizing the "time to peak" characteristics from observed flood events, and an added baseflow. However, these existing methods are inadequate or pose difficulties in several types of basins. These types include: very permeable limestone basins, basins including large lakes or sequences of lakes, or basins where a significant portion of streamflow in extreme flood events are caused by snowmelt. Snowmelt is a crucial contributor to flooding in the Naugatuck River basin. This study instead uses an alternative Synthetic Hydrograph method proposed by Archer et al. (2000). Archer et al. compare their method against FSR rainfall runoff method in two basins and find that the analysis is simpler and quicker. Their method provides much greater flood volumes associated with a flood peak discharge of specified return periods than approaches based on FSR rainfall runoff method. Additionally, the proposed method has the added benefit of not requiring the separation of base

flow and storm runoff as in other methods, but considering the hydrograph in its totality. For these enhancements the synthetic hydrograph method was preferred and employed here in.

The employed synthetic hydrograph method has five steps. First, from each annual maximum flood hydrograph, the duration of selected percentiles to peak flow was determined (Figure 3). Next, the durations before and after the peak were assessed separately to ensure that they represent a more realistic asymmetrical profile. For each percentile, median durations were derived using historical events of all magnitude. Then, the median duration was applied to synthesizing the hydrograph of an event of given return period. The historical events are extracted from USGS gauged observations automatically using the Characteristic Point Matching (CPM) method (Mei and Anagnostou, 2015). Finally, the sensitivity of the design hydrograph shape was tested in regards to flood magnitude. For full explanation of the method, review the "Methods" section in Archer et al. (2000). This method was used to construct synthetic hydrographs for flood events at 50, 100, 200, and 500-yr return periods used as upstream boundary conditions in river reach "A" for HEC-RAS modeling.

Hydraulic Simulation

In the preprocessing stage, topographic data required for flood inundation modeling by HEC-RAS was extracted from LIDAR derived DEM using an ArcGIS module called HEC-GeoRAS. First, a triangulated irregular network (TIN) was created from the LIDAR DEM. A TIN preserves the spatial variability of the original data because each horizontal and vertical position of the source data is captured at each triangle's vertices. Next, stream centerlines, river bank lines, predicted flow paths, inline structures, and river and terrain cross-sections were

digitized. In order to accurately capture the meandering river characteristics, cross-section spacing was less than 150 feet, and manual editing was made to ensure that no cross-sections intersected, and that each cross-section passed over the main channel line only once. Following digitization, channel central lines and cross-sections are encoded with z values from the TIN surface. These pre-processed river profiles are then exported to HEC-RAS to be used as a basis for hydraulic simulation. Two separate stream sections from the Naugatuck River were modeled and exported to HEC-RAS, one upstream section containing the Thomaston Dam (river reach "A"), and the other downstream section containing the critical electrical infrastructure (river reach "B") (Figure 4). Automated geo-processing tools like HEC-GeoRAS help streamline the geometric data preparation stage of simulation considerably.

Developed by the US Army Corps of Engineers, HEC-RAS is a popular 1D hydraulic model capable of solving the St. Venant water equations in 1D for unsteady flow. If the pre-processed geometric stream data and other specific flow boundary conditions are provided, HEC-RAS can compute water depth and velocity along the river reaches.

The next step was to construct the flood-control dam on the delineated flood plain by utilizing the high-resolution topographic data and supplementary building design information (gate characteristics, construction materials, etc.) gathered from correspondence with Thomaston Dam engineers. The Thomaston Dam controlling the upstream reach "A", is featured by two sluice gates, which is hoisted to limit the flow passing underneath. These gates are 5.66ft wide, can open to a maximum of 10 feet, and were assigned a typical energy loss coefficient of 0.6. Additionally, this dam is featured by a spillway 14 feet below the crest to reduce the pressure to the dam and release water in an extreme flooding scenario. In all tested flooding scenarios, flood

stages were far below the level to activate the spillway, and thus the spillway played no role in downstream inundation and will not be discussed in the scope of this paper.

For validation in extreme flooding conditions, we compared the simulation of the largest recent flood event in the region, occurring in late August 2011 as a result of hurricane Irene, against stage observation. The time period from August 27 to September 5 was picked out as one event. Peak flows for this event were on the order of 16,000 cfs. Hydrographs recorded by a stream-gage at the inlet to the dam was used for the model's upstream boundary condition. The measured flood-control gate height time-series from the Thomaston dam during this flood event were used as operation of the dam. Downstream the normal depth condition was set, with the friction slope estimated from the slope of the stream channel profile.

Subsequent to validation, multiple plans were simulated in the following flooding scenarios: a 50-year flood event, 100-year flood event, 200-year flood event, and 500-year flood event. In river reach "A", each simulation was forced by a corresponding synthetic hydrograph with the different initial depth conditions and gate operational plans. The plans include fully-open (10ft gate openings) and half-open gates (5ft gate openings). The conditions include under normal low flow (base flow conditions) and half-full. In the first condition, the dam is virtually empty when the simulation begins. In the second initial flow condition, the reservoir of the dam starts with 50% capacity filled. Water depths and stream velocities were finally output in a total of 16 flooding cases in the upper modeled river reach "A". The simulated hydrographs from river reach "A" were then added to the synthetic hydrographs of the same return period for river reach "B". The hydrographs were added "peak to peak", where the maxima of upstream hydrograph were combined directly with the maxima of downstream hydrograph with no delay time. This was done in order to simulate the "worst case scenario" of maximum flooding. The newly

altered synthetic hydrographs forced the hydraulic simulation in river reach "B". Depending on the flood scenario, the outflow from the dam contributed from 7-20% of the peak streamflow at the outlet of river reach "B" (Table 1), demonstrating the significance of accurate overland runoff simulation from the hydrological model. The final flood inundation results (water depths and velocities) were exported to HEC-GeoRAS for further post-processing and visualization.

HEC-GEORAS can also handle the hydraulic modeling outputs from HEC-RAS, importing them back into ArcGIS, graphically representing flood inundated areas over a digital terrain model. Post-processing methodology involves converting the model simulated water surface elevations and the pre-processed terrain elevations from TIN format to a GRID surface. These surfaces are then compared, and any cell in the flood plain where the water surface is higher than the terrain elevation is designated as flooded. The resultant flood extent maps were then placed over satellite imagery of the area for viewing purposes. This process was done for each of the HEC-RAS simulated flood scenarios.

5. Results

Validation of stream flow simulations

CREST-SVAS hydrologic model simulated stream flow in the watershed upstream of the Thomaston Dam. This discharge result was subsequently compared against observed discharges measured by a stream gauge at the inlet of the dam. A total of 45 events were simulated, with 9 of the events used for validation. A mosaiced hydrograph of all the events is presented in Figure 5. CREST-SVAS performed well in restoring these events. The Nash-Sutcliffe coefficient of efficiency (NSCE) is a normalized efficiency statistic frequently used to determine model

predictive accuracy. NSCE efficiencies range from negative infinity to one, with one indicating a perfect match (Nash and Sutcliffe, 1970). CREST-SVAS simulated streamflow's in the Naugatuck River basin had NSCE, correlation coefficient, and relative bias of water volume of 0.6997, 0.85, and -6.3%, respectively.

$$NSCE = 1 - \frac{\sum_{t=1}^{T}(Q_m^t - Q_o^t)^2}{\sum_{t=1}^{T}\left(Q_o^t - \overline{Q_o}\right)^2}$$

Q_o is the mean of observed discharges, Q_m is modeled discharge, and Q_o^t is observed discharge at time *t.*

Validation of hydraulic simulations

Simulated gate discharge from the August 27th 2011 flooding event in river reach "A" were validated against flow rates computed using gate ratings curves posted by the US Army Corps of Engineers (see Figure 6). During this event, a maximum flood stage of 74.66 ft was reached, producing gate discharges of 753 cfs and 1244 cfs when the gates were open 3ft and 5 ft, respectively. When compared to the flow rate computed by Thomaston Dam ratings curves, the model displayed good performance, with minor gate discharge discrepancies of only 77 cfs (10.23%) and 166 cfs (13.3%) for the two operational scenarios. Additionally, simulated stream flow rates for the same flooding event in river reach "A" were compared against observed hydrographs from a stream gauge (USGS station 01206900) residing 1.5 miles downstream of the Thomaston dam on the Naugatuck River (Figure 7). As seen in the figure, the model did well

in capturing the overall hydrograph shape; however, it consistently underestimated total streamflow. This underestimation is likely due to the gage's location. The gauge is 1.5 miles downstream to the outlet of the dam, and thus captures overland flow runoff occurring within this river section, in addition to the flows released from the dam. Overland runoff contribution from the watershed area in-between the dam and this stream gauge has not been taken into account in the simulation.

6. Discussion

Maximum inundation depth and extent maps simulated by the HEC-RAS model for each of the sixteen flooding cases in downstream river reach "B" are illustrated in Figures 8-11. Flood extent was determined by subtracting the underlying ground elevation from the LIDAR derived TINs from the water surface profile elevation. If the result was positive, then the area is classified as inundated and assigned a flood depth. Simulated water depths and extents have been co-displayed over satellite imagery to visualize the susceptibility of certain urban areas in Waterbury. A high-end limit of 7 feet was utilized in the inundation maps so that the spatial variability of flood depths could be more clearly represented. The majority of flood occurred in the floodplains on the eastern side of the Naugatuck River. An elevated highway that runs along the western edge of the river prevents floods from propagating in that direction.

Surprisingly, a portion of the electrical substation, more specifically the outside transformers, are partially or fully inundated in all flood scenarios. The maximum flood depth in each scenario at the outside transformer are well as the enclosed building complex can be seen in Table 2. The probability of the flooding event, or peak flood magnitude, played the most

significant role in controlling maximum water depth at the substation. As expected, flood severity increased with decreasing flood probability, with the largest flood depths and extents occurring during lowest probability, highest magnitude flood events. During the "worst case scenarios", a 500-year flood with the upstream dam's revivor initially half-filled and both flood control gates fully-open, the substation experienced an estimated 4.63 and 2.69 feet of inundation at the outside transformers and complex, respectively. In all scenarios the transformers were more severely affected by flooding than the building itself, likely due their close proximity to the river's bank.

This study also examined how different flood infrastructure management strategies helped to protect downstream floodplain areas. The manipulation of the flood control dam's gate height had a recognizable influence on both estimated maximum flooding extent and flood depth. This influence was more substantial during the 50-year and 100-year higher probability flooding events. With an initially empty dam reservoir, moving from half open to fully open gates produced 165%, 90%, 7%, and 6% increases in maximum water depth at the transformer for the 50-, 100, 200, and 500- return period simulated extreme flood events. While the building complex was dry for the 50- and 100-year flood scenarios, it too saw increases of 33%(200-year) and 21%(500-year) in flood depth when simulated with the same initial empty reservoir conditions.

Comparing the simulated results from model runs with and without an initially filled reservoir illuminates the dam's ability to dampen the flooding effects in downstream floodplains when hit with a large amount of water from two extreme events in close temporal proximity. The dam is outfitted with two sluice gates to control flows. These gates sit at the bottom of the channel in the dam's reservoir. As the flood stage in the reservoir upstream of the dam grows

larger, so does the pressure from the water columns weight above the gate, resulting in larger streamflow's output from the dam. During an extreme event this extra water will likely finds its way over the banks and into the downstream floodplain. These results can be seen in Table 2. Much like the relationship between gate height and maximum water depth and inundation extent, increased effects are found during higher probability, more frequent flood events. When changing from an initially empty reservoir to an initially half-filled reservoir, the model predicted increases in maximum water depth at the transformer of 10% and 63% for a 50-year flood, and increases of 24% and 29% for a 100-year flood, in maximum water depth at the transformer with gates half and fully-open, respectively. The increases during lower probability extreme events are less severe, resulting in only increases of only 6%, 5%, 5%, and 8% (200-year half and fully, 500-year half and fully) maximum water depth at the outside transformer. The initial reservoir stage affected not only water depth, but increased the inundation extent which can be seen in all of the inundation maps.

The results from our study indicated that initial water levels in the dam's reservoir served as a major factor in controlling simulated inundation extent and water levels depths. Similar to the trends with gate height, these effects are more significant in more frequent floods with higher probability (50- and 100-year), increasing maximum simulated water depths at the transformer by 10%, 63%, 24%, and 29% for the 50-year flood return period.

7. Conclusion

Accurate information regarding flood depth and inundation extent are invaluable to the assessment of potential flood risk. Flood inundation maps are a vital tool used in flood

management policy to help improve resilience in flood prone areas, especially in floodplains holding critical. The reliability of these maps however is directly depended on the accuracy and availability of the input data used to create them. Unfortunately, in some regions of the U.S., like ungauged watersheds, this data can be lacking and these areas can be put under unnecessary increased risk.

In this paper we present a comprehensive framework aimed at improving flood resilience by producing flood inundation maps for future extreme event scenarios for the Naugatuck River in Connecticut. Our methodology links flood frequency analysis with a physically based, fully distribution hydrologic model, and a one-dimensional unsteady hydraulic model. To ensure model reliability and performance in potentially ungauged basins, we utilized observation corrected, long term, NLDAS meteorological forcing data, a novel methodology using measured streamflows to create synthetic hydrographs, and fine resolution LIDAR terrain elevation data to construct accurate stream channel profiles. Additionally, our chosen study area features two critical infrastructures, an upstream flood control dam with two sluice gates and a downstream electric substation. Historic gate-height time series as well as other various dam construction specifics gathered from correspondence with dam engineers were used to assure the successful recreation of the dam in the model. Our validation process was twofold. First, the simulated streamflows from the CREST-SVAS hydrologic model was validated against flowrates measured at a stream gauge at the inflow of the dam. Secondly, the streamflow results from the HEC-RAS hydraulic model were validated against gate ratings curves at the dam as well as against measured streamflow results from a gauge downstream of the dam. Ultimately, our framework was employed to investigate flood hazard by creating flood inundation maps for the Naugatuck

River at a critical infrastructure under four separate extreme flood events (50-,100-,200-,500-year return periods), two separate dam operation procedures (gates half- and fully-open), and two separate initial dam reservoir conditions (empty revivor and half-filled reservoir), resulting in a total of 16 flood cases. These inundation maps were combined with satellite imagery to better represent the extent of flooding and potential areas affected.

8. References

Aerts, E.A., (2014) Climate adaptation. Evaluating flood resilience strategies for coastal megacities. Science 344(6183):473–475

Ahearn, E., 2003. *Peak-Flow Frequency Estimates for U.S. Geological Survey Streaflow-Gaging Stations in Connecticut,* East Hartford, CT: U.S. Geological Survey Water-Resources Investigations Report 03-4196

Ahearn, E.A., 2004, Regression equations for estimating flood flows for the 2-, 10-, 25-, 50-, 100-, and 500-year recurrence intervals in Connecticut: U.S. Geological Survey Scientific Investigations Report 2004–5160, 62 p.

Ahearn, E.A., 2005, Estimates of the Magnitude and Frequency of Flood Flows in the Connecticut River in Connecticut: U.S. Geological Survey Open File Report 2005–1369, 12 p.

Ahearn, E.A., 2009, Flood of April 2007 and flood-frequency estimates at streamflow-gaging stations in western Connecticut: U.S. Geological Survey Scientific Investigations Report 2009-5108, 40 p. Available online only at http://pubs.usgs.gov/sir/2009/5108.

Archer, D., Foster, M., Faulkner, D., Mawdsley, J., 2000. The synthesis of design flood hydrographs, Proc. ICE/CIWEM Conf. Flooding–Risks and Reactions. Terrace Dalton, London.

Baldwin, M., and K.E. Mitchell, 1997: The NCEP hourly multi-sensor U.S. precipitation analysis for operations and GCIP research. Preprints, 13th AMS Conference on Hydrology, pp. 54-55, Am. Meteorol. Soc., Boston, Mass.

Bales, J.D., Wagner, C.R., Tighe, K.C., and Terziotti, Silvia, 2007, LiDAR-derived flood-inundation maps for real-time flood-mapping applications, Tar River basin, North Carolina: U.S. Geological Survey Scientific Investigations Report 2007–5032, 42 p.

Bao, Z., Zhang, J., Liu, J., Fu, G., Wang, G., He, R., et al., 2012. Comparison of regionalization approaches based on regression and similarity for predictions in ungauged catchments under multiple hydro-climatic conditions. J. Hydrol. 466– 467 (21), 37–46.

Bates, P.D., Wilson, M.D., Horritt, M.S., Mason, D.C., Holden, N., and Currie, A., 2006, Reach-scale floodplain inundation dynamics observed using airborne synthetic aperture radar imagery—Data analysis and modelling: Journal of Hydrology, v. 328, p. 306–318.

Cea, L., Garrido, M., Puertas, J., 2010. Experimental validation of two-dimensional depth-averaged models for forecasting rainfall-runoff from precipitation data in urban areas. J. Hydrol. 382 (1–4), 88–102.

Charlton, M. E., Large, A. R. G., & Fuller, I. C. (2003). Application of airborne LiDAR in river environments: The River Coquet, Northumberland, UK. Earth Surface Processes and Landforms, 28(3), 299–306. doi:10.1002/esp.482

Chow, V. T., 1951. A general formula for hydrologic frequency analysis. *Transactions American Geophysical Union,* 32(2), pp. 231-237

Chow, V., Maidment, D. & Mays, L., 1988. *Applied Hydrology.* International Editions ed. Singapore: McGraw-Hill

Cook, A., Merwade, V., 2009. Effect of topographic data, geometric configuration and modelling approach on flood inundation mapping. J. Hydrol. 377, 131–142. http://dx.doi.org/10.1016/j.jhydrol.2009.08.015.

Coveney S, Fotheringham AS (2011) The impact of DEM data source on prediction of flooding and erosion risk due to sea-level rise. International Journal of Geographical Information Science 25: 1191–1211.

Daly, C., R.P. Neilson, and D.L. Phillips, 1994: A statistical-topographic model for mapping climatological precipitation over mountainous terrain. *J. Appl. Meteor.*, 33, 140-158, doi:10.1175/1520-0450(1994)033<0140:ASTMFM>2.0.CO;2

Dis, M., Anagnostou, E., Zac, F., Vergara, H., Hong, Y., 2015. Evaluating multi-scale flow predictions for the Connecticut River Basin. Hydrol:. Curr. Res. 6 (2), 1. Geological_Survey, US, 2009. USGS Surface-Water Data for USA.

Gueudet, P., Wells, G., Maidment, D.R., Neuenschwander, A., 2004. Influence of the postspacing density of the LiDAR-derived DEM on flood modeling. Geographic Information Systems and Water Resources III — AWRA Spring Specialty Conference. AWRA, Nashville, Tennessee.

Haan, C., 1977. *Statistical methods in Hydrology.* Ames, Iowa, USA: Iowa State University Press.

Higgins, R.W., W. Shi, E. Yarosh, and R. Joyce, 2000: Improved United States precipitation quality control system and analysis. NCEP/Climate Prediction Center Atlas No. 7.

Hilldale, R. C. and Raff, D. (2008), Assessing the ability of airborne LiDAR to map river bathymetry. Earth Surf. Process. Landforms, 33: 773–783. doi:10.1002/esp.1575

Hirabayashi, Y., et al., 2013. Global flood risk under climate change. Nature Climate Change, 3, 816–821. doi:10.1038/nclimate1911

Hydrologic Engineering Center, 2002, HEC–RAS river analysis system user's manual, version 3.1: Davis, CA, U.S. Army Corps of Engineers Computer Program documentation report 68; accessed August 30, 2006, at http://www. hec.usace.army.mil/software/hec-ras/hecras-document.html [variously paged].

Julien, P.Y., Saghafian, B., Ogden, F.L., 1995. Raster-based hydrologic modeling of spatially-varied surface runoff. Water Resour. Bull. 31 (3), 523–536.

Kim, J., Warnock, A., Ivanov, V.Y., Katopodes, N.D., 2012. Coupled modeling of hydrologic and hydrodynamic processes including overland and channel flow. Adv. Water Resour. 37, 104–126.

Li, Z., Yang, D., Gao, B., Jiao, Y., Hong, Y., Xu, T., 2015. Multiscale hydrologic applications of the latest satellite precipitation products in the Yangtze River basin using a distributed hydrologic model. J. Hydrometeorol. 16 (1), 407–426.

Loukas, A., Vasiliades, L., 2014. Streamflow simulation methods for ungauged and poorly gauged watersheds. Nat. Hazards Earth Syst. Sci. 14 (7), 1641–1661.

Mei, Y., Anagnostou, E.N., 2015. A hydrograph separation method based on information from rainfall and runoff records. J. Hydrol. 523, 636–649. http://dx.doi.org/10.1016/j.jhydrol.2015.01.083.

Nash, J. E. and Sutcliffe, J. V.: River flow forecasting through conceptual models, Part I - A discussion of principles, J. Hydrol., 10, 282–290, 1970.

NERC, 1975. *Flood Studies Report*, Volumes I-V, Natural Environment Research Council, London, UK.

Omer, C.R., Nelson, J., Zundel, A.K., 2003. Impact of varied data resolution on hydraulic modeling and floodplain delineation. Journal of the American Water Resources Association 39, 467–475.

Parr, D., Wang, G., Bjerklie, D., 2015. Integrating remote sensing data on evapotranspiration and leaf area index with hydrological modeling: impacts on model performance and future predictions. J. Hydrometeorol. 16 (5), 2086–2100.

Qu, Y., Duffy, C.J., 2007. A semidiscrete finite volume formulation for multiprocess watershed simulation. Water Resour. Res. 43 (8).

Razavi, T., Coulibaly, P., 2012. Streamflow prediction in ungauged basins: review of regionalization methods. J. Hydrol. Eng. 18 (8), 958–975.

Schinke, R.; Kaidel, A.; Golz, S.; Naumann, T.; López-Gutiérrez, J.S.; Garvin, S. Analysing the Effects of Flood-Resilience Technologies in Urban Areas Using a Synthetic Model Approach. *ISPRS Int. J. Geo-Inf.* **2016**, *5*, 202.

Schumann, G., Matgen, P., Cutler, M. E. J., Black, a., Hoffmann, L., & Pfister, L. (2008). Comparison of remotely sensed water stages from LiDAR, topographic contours and SRTM. ISPRS Journal of Photogrammetry and Remote Sensing, 63(3), 283–296. doi:10.1016/j.isprsjprs.2007.09.004

Shen, X., Hong, Y., Zhang, K., Hao, Z., 2016. Refining a distributed linear reservoir routing method to improve performance of the CREST model. J. Hydrol. Eng. 04016061.

Shen, X., Anagnostou, E., 2017. A Framework to Improve Hyper-Resolution Hydrologic Simulation in Snow-Affected Regions", *Journal of Hydrology, vol.552, pp.1-12*, DOI:10.1016/j.jhydrol.2017.05.048.

Tasker, G. D., 1978. Flood Frequency Analysis with a Generalized Skew Coefficient. *Water Resources Research*, 14(2), pp. 373-376.

U.S. Water Resources Council, C. o. W., 1981. *Guidelines for determining flood flow frequency, bulletin 17B*, Reston, VA: U.S. Geological Survey.

USDA Soil Conservation Service, 1986, Urban Hydrology for Small Watersheds. Technical Release 55, 2nd ed., NTIS PB87-101580, Springfield, VA.

Vivoni, E., Entekhabi, D., Bras, R., Ivanov, V., 2007. Controls on runoff generation and scale-dependence in a distributed hydrologic model. Hydrol. Earth Syst. Sci. 11 (5).

Wang, Y., Zheng, T., 2005. Comparison of light detection and ranging and National Elevation Dataset digital elevation model on floodplains of North Carolina. Natural Hazards Review 6, 34–40.

Wang, J., Hong, Y., Li, L., Gourley, J.J., Khan, S.I., Yilmaz, K.K., et al., 2011. The coupled routing and excess storage (CREST) distributed hydrological model. Hydrol. Sci. J. 56 (1), 84–98.

Xiong, L., Du, T., Xu, C.Y., Guo, S., Jiang, C., Gippel, C.J., 2015. Non-stationary annual maximum flood frequency analysis using the norming constants method to consider non-stationarity in the annual daily flow series. Water Resour. Manage, 1–19.

Xue, X., Hong, Y., Limaye, A.S., Gourley, J.J., Huffman, G.J., Khan, S.I., et al., 2013. Statistical and hydrological evaluation of TRMM-based Multi-satellite Precipitation Analysis over the Wangchu Basin of Bhutan: Are the latest satellite precipitation products 3B42V7 ready for use in ungauged basins? J. Hydrol. 499, 91–99.

Figures and Tables

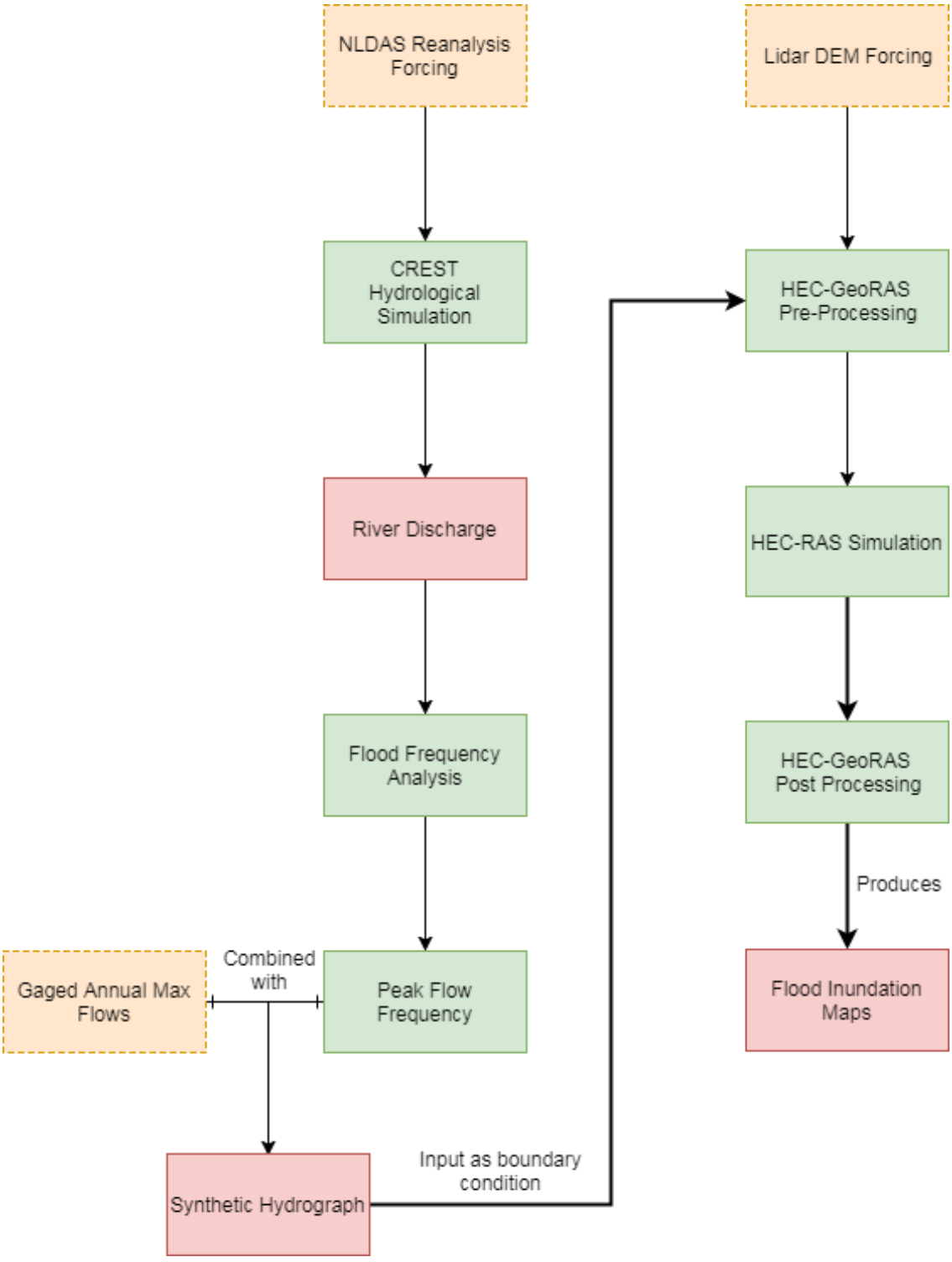

Figure 1- Structure of model integration

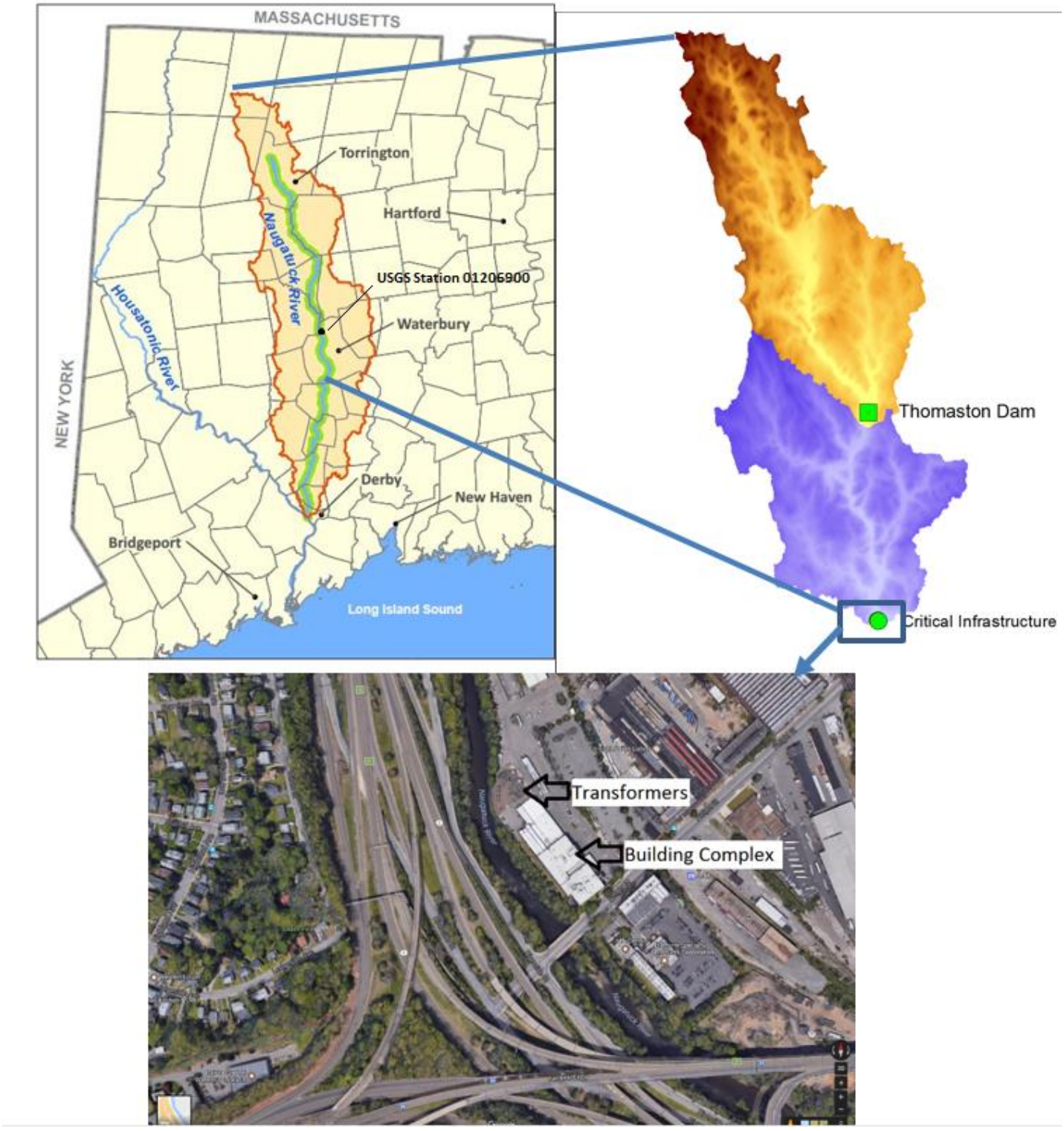

Figure 2- a) The Naugatuck River Basin, b) the subdivision of the Naugatuck River Basin, c) satellite imagery of electrical substation in Waterbury, Connecticut

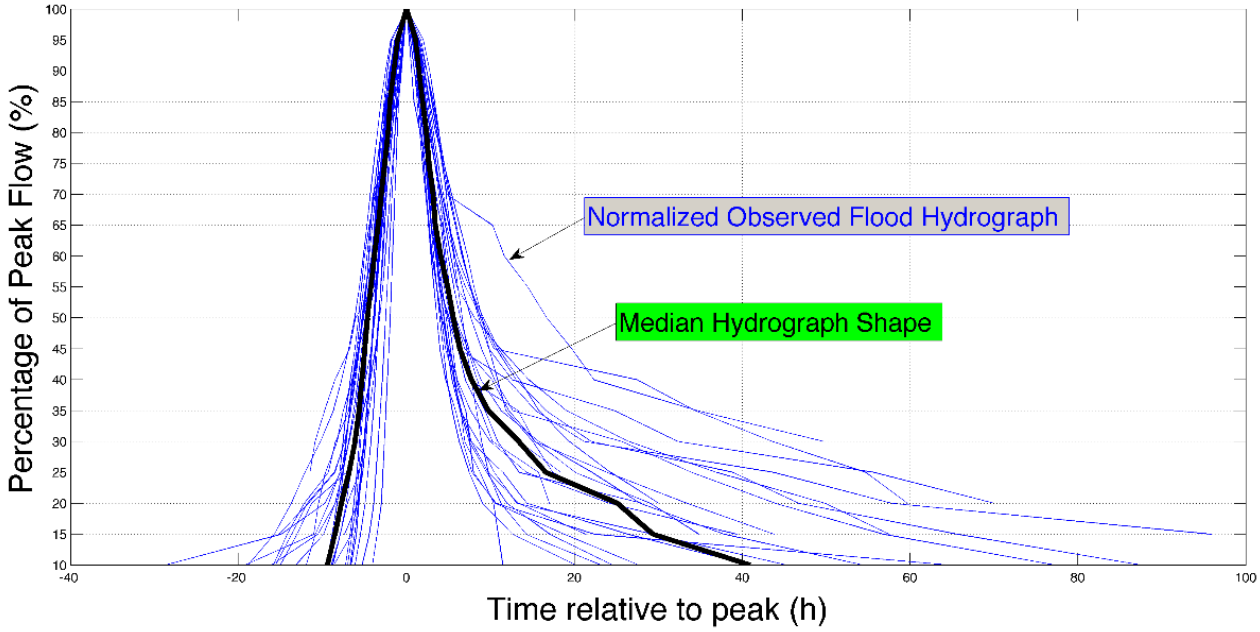

Figure 3- Deriving median durations for each exceedance percentile to determine median hydrograph shape

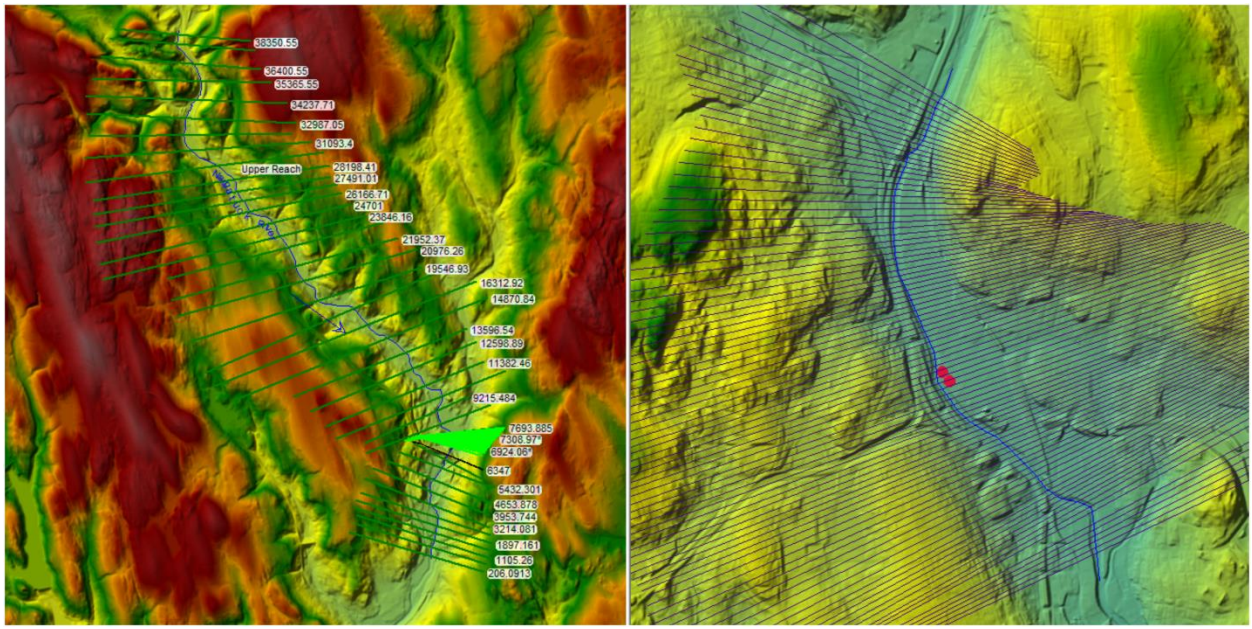

Figure 4-Upstream river reach "A" and downstream river reach "B" modeled in the HEC-RAS domain displayed over LIDAR derived DEM

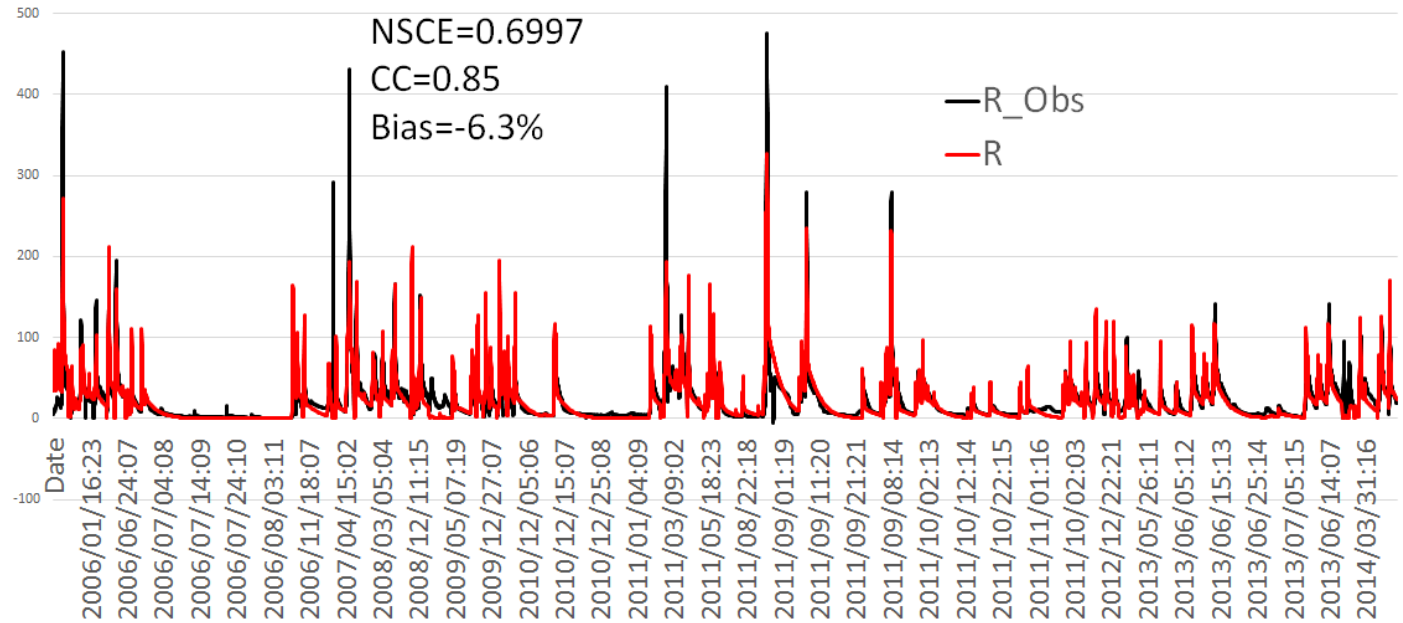

Figure 5- CREST-SVAS daily streamflow validation against observation for Naugatuck River Basin at inlet of Thomaston Dam

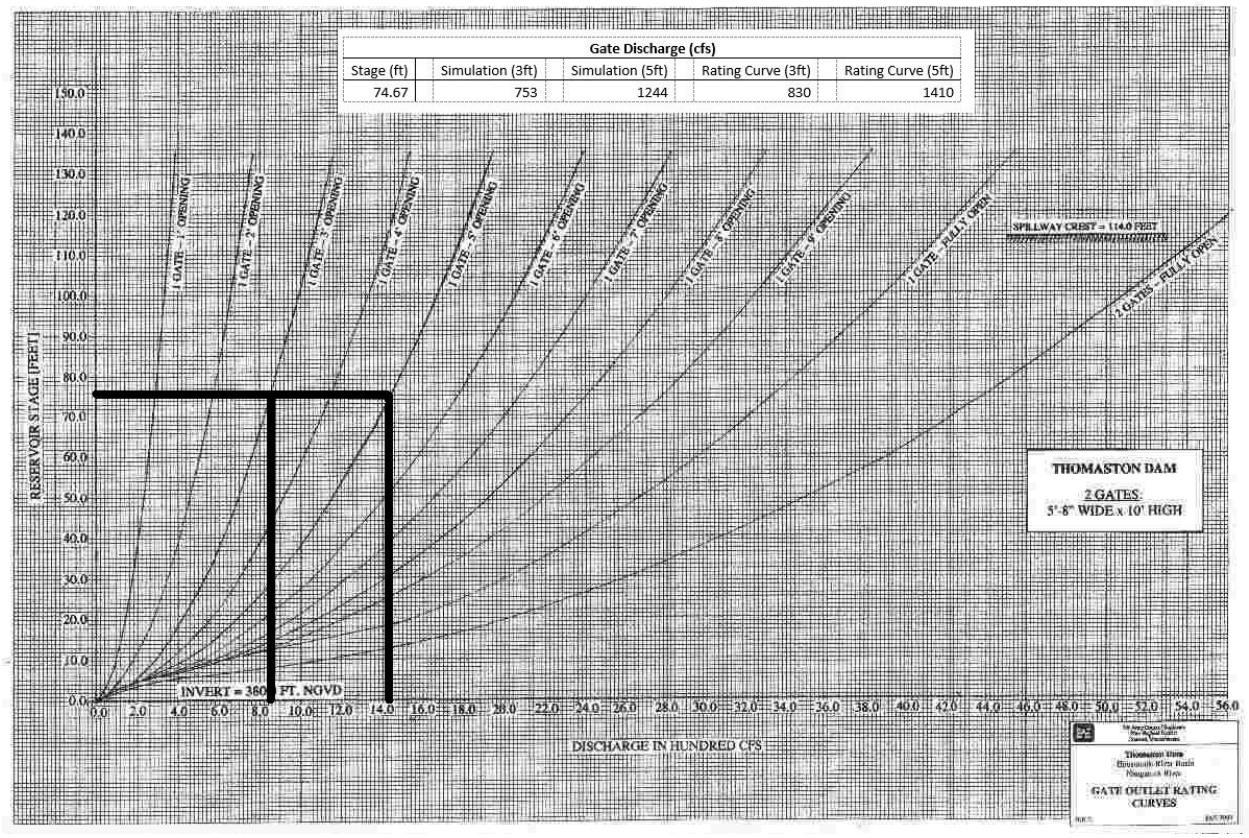

Figure 6- Model simulated gate discharge validated against Thomaston Dam posted ratings curves

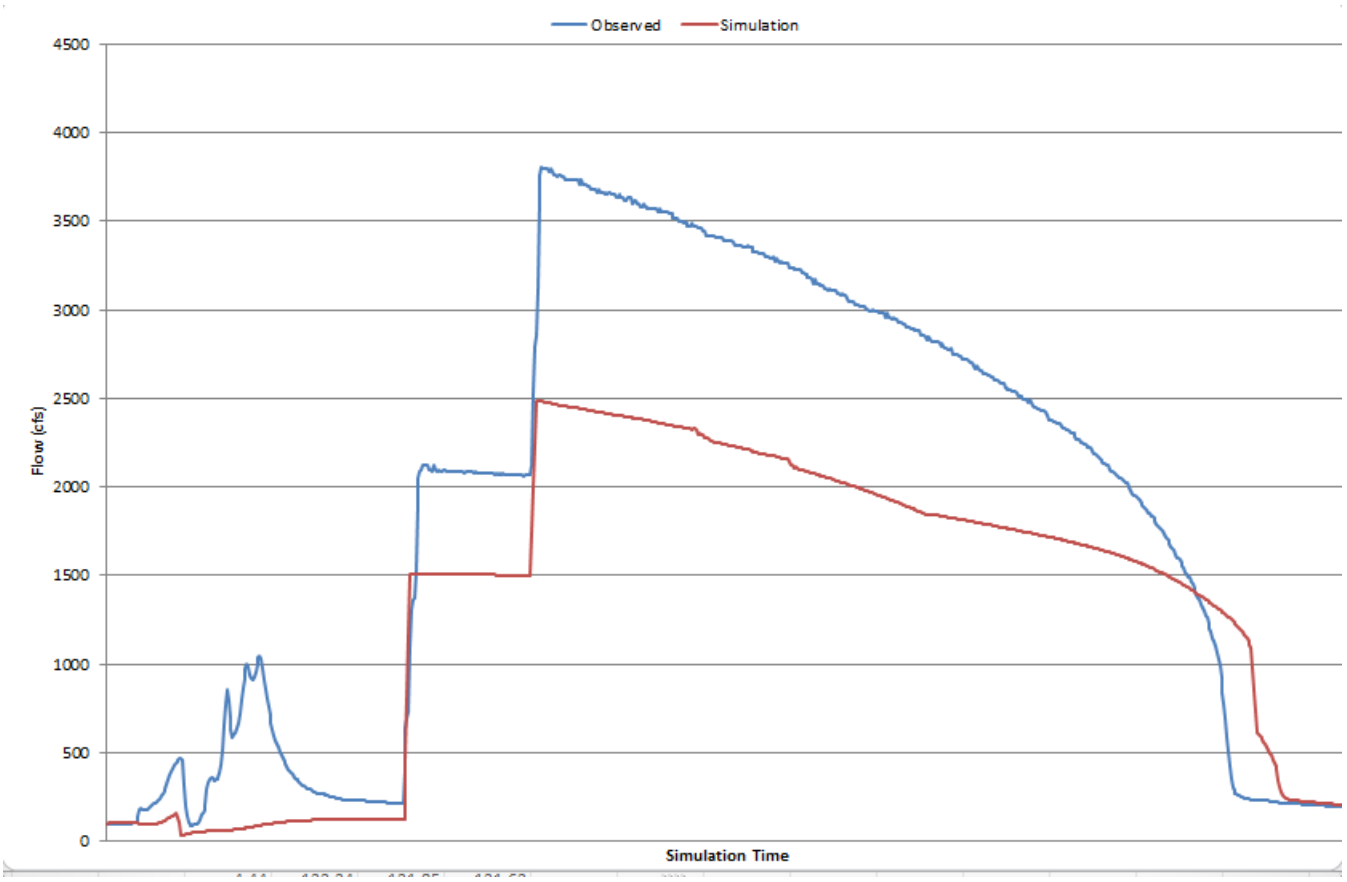

Figure 7- Model simulated dam output streamflow validated against observations from USGS station 01206900 Naugatuck River at Thomaston, CT

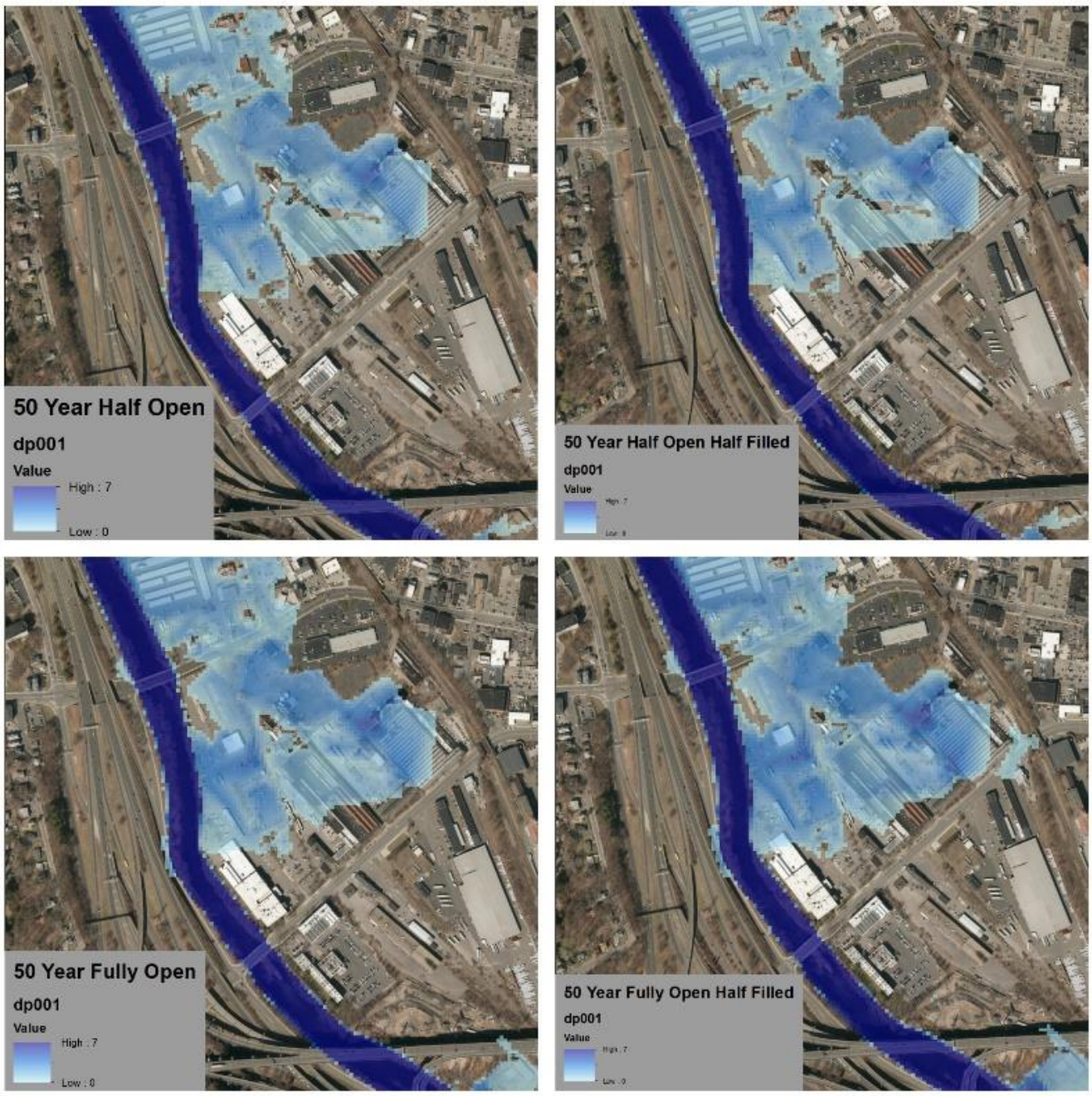

Figure 8- Simulated maximum 50-year flood inundation in various dam operation scenarios at an ungaged reach

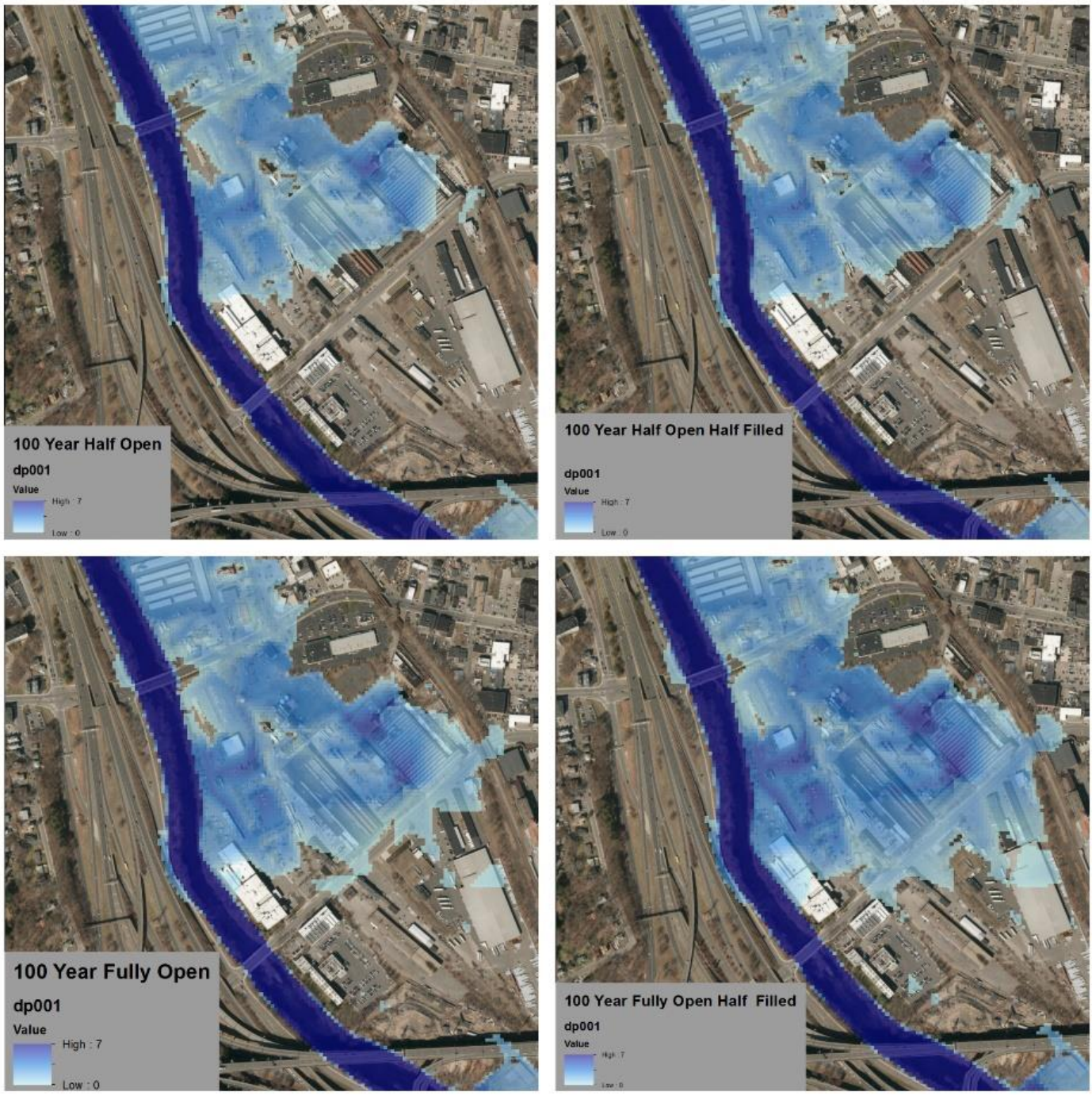

Figure 9- Simulated maximum 100-year flood inundation in various dam operation scenarios at an ungaged reach

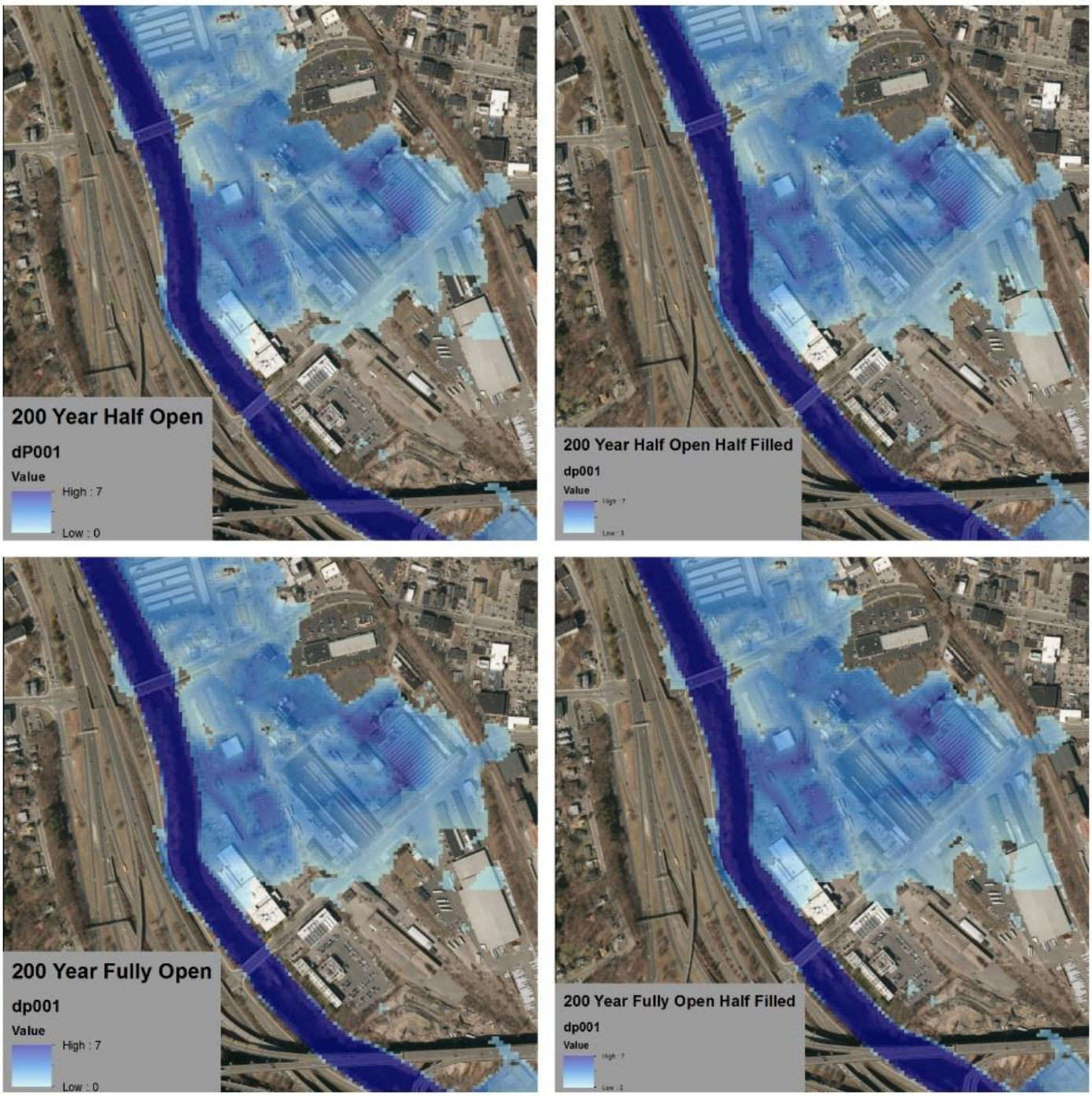

Figure 10- Simulated maximum 200-year flood inundation in various dam operation scenarios at an ungaged reach

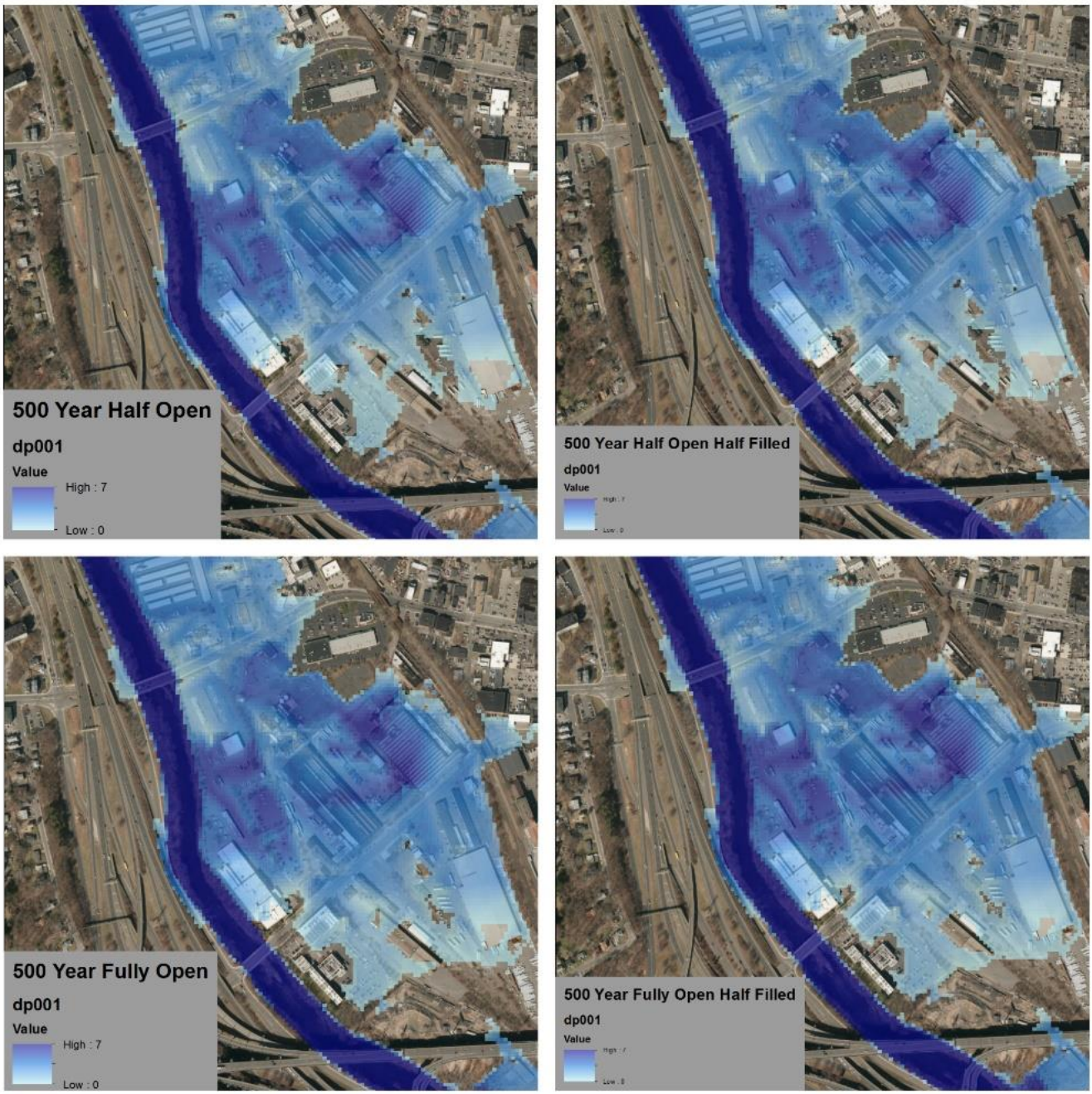

Figure 11- Simulated maximum 500-year flood inundation in various dam operation scenarios at an ungaged reach

Dam Peak Streamflow Contribution (cfs)		
Flooding Scenario	Half Open	Fully Open
50 Year		
Empty Reservoir	22930 (9.94%)	24890 (16.90%)
Half Filled Reservoir	23369 (11.52%)	25862 (20.07%)
100 Year		
Empty Reservoir	25514 (9.20%)	27558 (15.78%)
Half Filled Reservoir	25922 (10.52%)	28453 (18.45%)
200 Year		
Empty Reservoir	28168 (8.56%)	30289 (14.80%)
Half Filled Reservoir	28549 (9.67%)	31116 (17.07%)
500 Year		
Empty Reservoir	31810 (7.83%)	34024 (13.68%)
Half Filled Reservoir	32161 (8.73%)	34776 (15.52%)

Table 1- Thomaston Dam outflow contribution to downstream peak streamflow

	Maximum Water Depth (feet)	
Flooding Scenario	**Outside Transformer**	**Building**
50 Year		
Half Open	0.40	0.00
Half Open Half Filled	0.44	0.00
Fully Open	1.06	0.00
Fully Open Half Filled	1.73	0.00
100 Year		
Half Open	1.37	0.00
Half Open Half Filled	1.70	0.00
Fully Open	2.60	0.26
Fully Open Half Filled	3.36	1.29
200 Year		
Half Open	3.10	1.04
Half Open Half Filled	3.30	1.34
Fully Open	3.33	1.39
Fully Open Half Filled	3.51	1.55
500 Year		
Half Open	4.01	2.12
Half Open Half Filled	4.20	2.22
Fully Open	4.28	2.57
Fully Open Half Filled	4.63	2.69

Table 2- - Maximum water depth (ft) at critical infrastructure in an ungaged reach.